CR-128534

QUANTITATIVE MICRO-LUMINESCENCE AND RELATED STUDIES OF FINE AND/OR GLASSY LUNAR SURFACE MATERIALS

NGR-
Grant No. 39-009-183

Principle Investigator

Rustum Roy

Interim Technical Report for the Period

March 1, 1971 - February 29, 1972

To

National Aeronautics and Space Administration
Office of Science and Technical Information
Washington, D.C. 20546

THE MATERIALS RESEARCH LABORATORY

THE PENNSYLVANIA STATE UNIVERSITY

UNIVERSITY PARK, PENNSYLVANIA

June 15, 1972

Proceedings of the Third Lunar Science Conference
(Supplement 3, *Geochimica et Cosmochimica Acta*)
Vol. 1, pp. 0000–0000
The M.I.T. Press, 1972

Structure of lunar glasses by Raman and soft x-ray spectroscopy

GEORGE W. FABEL, WILLIAM B. WHITE, EUGENE W. WHITE, and RUSTUM ROY
Materials Research Laboratory,
The Pennsylvania State University,
University Park, Pennsylvania 16802

Abstract— X-ray spectra and Raman spectra have been measured from individual particles of lunar glasses. Each particle was analyzed separately by electron microprobe. Silicon emission shifts vary between parent rock types and can be interpreted as a range of Si–O distances from 1.612 to 1.637A. Aluminum emission shifts relate to the amount of 4- and 6-coordinated Al in the glass. Raman spectra show broadened bands. Certain bands recur in many specimens and relate to the main normative minerals for the glass bulk composition, olivine, pyroxene, and anorthite.

INTRODUCTION

THE VERY LARGE NUMBER of chemical analyses now available for glass particles and lithic fragments in the lunar soils cluster into distinct populations that permit the identification of the same number of lunar rock types. Various classifications have been proposed. We have adapted the work of Reid *et al.* (1972) to classify the glass particles examined in our investigation. It seems to be recognized that the composition of the glass particles also Hirrors an average composition of parent rock types or individual lunar minerals with little modification during melting and transport. There are, therefore, a number of kinds of lunar glass, identifiable by their chemical composition. Our objectives in the present paper are to relate as far as possible the structure-sensitive parameters of these glasses to their chemical composition.

The approach is to measure Raman spectra and x-ray emission spectra on individual glass particles. Electron microprobe analyses of the same particles permit correlation of each particle with a known composition, and the interpretation of the structural measurements can be made on this basis.

EXPERIMENTAL METHODS

Selection and mounting of specimens

A representative assortment of glass particles was selected under an optical microscope from Apollo 11–15 fines. These glassy specimens consisted primarily of opaque spherules, opaque glass coatings on rock fragments, and angular fragments of transparent and opaque glass. With the exception of three large specimens (15017.9, 15245.56, and 15015.26, all ~2 cm across), particle size ranged from 0.3 to 2 mm. All specimens were prepared as polished grain mounts using Koldmount self-curing resin. For the three large samples, small glass fragments (~3 mm) were broken off and mounted.

Chemical analysis

The chemical analyses shown in Table 1 were obtained with an Applied Research

Laboratories (ARL) electron microprobe. When two glass standards are used, results are good to approximately ±10% relatively. The specimens were first checked for chemical homogeneity by scanning the electron beam over a 360 × 360 μ area and observing the absorbed electron image. The samples were found to fall into

Table 1. Microprobe analyses (wt%) of

Sample number	SiO_2	Al_2O_3	CaO	MgO	FeO
10084,110,1A	49	20	15	9.6	4.7
10084,110,1B	48	22	16	9.6	4.8
10084,110,2,8	50	23	14	7.8	4.5
10084,110,2,9	56-57	25-28	14-19	<0.1	<0.1
	53-58	0-2	3-18	15-40	7-12
10084,110,1H	51-57	17-21	12-18	2-5	0-6
	29-56	9-18	1-12	8-17	6-23
10084,110,3,1	48-55	8.5-10	10-11	8-8.5	15-15.5
12070,42-1	52-61	11-19	1.5-8.5	3.5-11	10-14.5
12070,42-2	46-58	2-26	6-15	8-21	6-19
12070,42-3	55-65	0-4	5-17	8-21	12-27
12042,32-1	50	19	14	10.7	5.1
12042,32-2	42-63	2.5-13.5	5-14.5	2-10.5	4-16.5
12042,32-3	34-49	31-35	0-0.5	0-0.5	0.5-1.5
	46-54	0.5-3.0	3.5-7.0	16-21	14-21
12042,32-4	34-49	27-33	13-17	0-2.5	0.5-3
	14-44	2-13	3-9.5	6-25	18-29
14162,47-1	46	25	14	9.5	5.2
14162,47-2B	46-58	2-26	6-15	8-21	6-19
14162,47-2C	42-60	36-39	15-18	<0.1	0-2
	58-62	0-7	3-8	15-21	10-24
14162,47-3	45-53	32-38	10-15	0-1.5	0-1
	34-58	6-13	2-7	18-30	19-35
14162,47-5	45-49	32-38	13-17	0-1	0-2
	37-55	3-10	3-7	18-23	11-20
14162,61-1	50	18	10	9.8	6.3
14162,61-2	46-53	16-22	12-17	0-1	0-3
	44-51	9-12	5-11	9-12	4-3
14162,61-3	43-43	14-42	8-14	--	0-7
	44-50	5-12	2-5	20-23	9-15
14162,61-4	41-50	31-32	15-17	0.5-2	0-1
	32-44	0.1	0.2	28-34	27-28
14162,61-5	43-60	19-36	11-17	--	0-4
	46-54	7-12	4-7	16-22	7-11
15501,25	42-50	9-11	8-10	11-12	14-16
15531,40	39-43	<0.1	0-0.3	27-31	25-30
15231,49-1	44-50	15.5-19.5	12.5-14	7.5-11	8.5-11.5
15231,49-2	42-40	22-29	11-18	1.5-5.5	2.5-7.5
	47-59	4-13	9-13	8-13	9-19
15231,49-3	42-50	11-16	10-16	--	12-16
	43-68	0.5-1.0	5-12	13-16	15-25
15015,26	44-47	23-35	11-16	0-7.5	0.5-8.5
	43-61	0-8.5	0.5-12	16-31	13-24
15245,56	32-42	30-39	16-20	<0.1	0-3.5
	57-69	0-2	1-6.5	22-32	10-11
15017,9	25-58	7.5-12.5	9.5-10.8	7.7-11.8	9-13.2

three principal categories: (1) homogeneous, (2) heterogeneous with no clear phase separation, and (3) heterogeneous with separation into Al, Ca zones and Fe, Mg zones. With some care it was possible to focus the electron beam into each zone and obtain individual chemical analyses as shown in Table 1.

lunar glasses used for spectral measurements.

TiO_2	K_2O	Form	Color	Homogeneity*	Rock type†
—	0.1	Shard	Clear green	H	H
—	0.1	Shard	Clear green	H	H
—	0.1	Vesicular	Clear yellow	H	H
<0.1	<0.1	Shard	Clear brown	IH	H-M
0–0.5	<0.1				
0–2.5	<0.1	Vesicular	Black	IH	H-M
0–1.5	<0.1				
4.5–5.5	<0.1	Shard	Black	H	M
0.5–2	0.2–1.0	Spatter	Brown-black	IH	K
0.5–3.5	0–0.2	Spatter	Brown-black	IH	M
0.5–1.5	<0.1	Spatter	Brown-black	IH	M
<0.2	<0.1	Shard	Clear green	H	H
0–2.5	0–0.8	Sphere	Black	IH	M
<0.1	<0.1	Spatter	Clear yellow	IH	A-M
0–1	<0.1				
0–1	<0.1	Spatter	Brown-black	IH	A-M
0.5–11	0–0.2				
0.2	0.1	Shard	Brown-black	H	H
0.5–3.5	0–0.2	Vesicular	Brown-black	IH	K
<0.1	<0.1	Vesicular	Brown-black	IH	A-M
0–0.5	0–0.2				
—	—	Vesicular	Brown-black	IH	A-M
—	—				
—	—	Vesicular	Brown-black	IH	A-M
—	—				
1.7	0.3	Sphere	Black	H	K
0–1	0–0.3	Ropy strand	Brown-black	IH	K
3–5	0–0.5				
0–1	0–0.4	Shard	Brown-black	IH	K
4–7	<0.1				
0–0.2	0–0.3	Vesicular	Brown-black	IH	A-M
0–0.5	<0.1				
0–2	0–1	Vesicular	Brown-black	IH	A-K
0–2	0–0.2				
1.0–1.5	0–0.2	Ropy strand	Brown-black	H	M
<0.1	0.1	Shard	Brown	H	M
0.5–1	0.1	Sphere	Brown-black	H	K-M
0.1–0.6	0–0.3	Vesicular	Black	IH	H-K
0.5–1.5	0–0.4				
—	0–0.2	Vesicular	Brown-black	IH	M
0.5–1.0	<0.1				
0–0.5	<0.1	Glazed rock	Brown	IH	A-M
0–0.5	0–0.2				
<0.1	<0.1	Spatter	Brown-black	IH	A-M
0–0.3	<0.1				
0.9–1.2	0.2–0.6	Spatter	Brown-black	IH	K

*H = homogeneous; IH = inhomogeneous.

†Rock types are: M = Mare basalts undifferentiated; K = Fra Mauro (KREEP) basalts; H = Highland basalts; A = Anorthosite composition.

Emission shifts

The AlK_β, SiK_β, and OK_γ x-ray emission bands were recorded for all specimens using an ARL electron microprobe model EMX operated at 20 keV and a specimen current of 0.10 to 0.30 μA. An ADP crystal was used for resolving the AlK_β and SiK_β, and clinochlore was used for the OK_γ. The peak shift was measured from 2/3 height position. The SiK_β and OK_γ emission shifts (Δ) were measured with respect to an α-quartz standard and the AlK_β with respect to α-Al_2O_3. The microprobe was operated with a large spot diameter of $\sim 100\ \mu$. The spectra were measured at several points on each sample. The shift (Δ) is defined here as

$$\Delta = \lambda\,(\text{specimen}) - \lambda\,(\text{standard}).$$

The precision of the shaft measurements is about $\pm 10\%$. Details of the experimental procedure employed here are reported elsewhere (White and Gibbs, 1967, 1969, and Gigl *et al.*, 1970).

Raman spectra

The Raman spectra of the mounted specimens were measured using a Spex Ramalog double grating spectrometer. Excitation was provided by the 488 or 514.5 nm line of an ionized-argon laser source with a power output of approximately 200 mW. The sample was positioned at the focal point of the laser beam and the Raman scattered light observed at 90° to the incident direction. Because the laser beam can be focused to a diameter less than 0.1 mm, it was possible to record spectra at several different points on each specimen. In a few instances, spectra from the specimen mounting material (Koldmount) were superimposed on the glass spectra. However, this was easily subtracted out.

Raman spectra of some particles, particularly those measured directly on unmounted and unpolished glass fragments, exhibited considerable sharp fine structure in the low-frequency region. Prolonged investigation has identified at least three sources for the fine structure:

1. Phase separation resulting in regions of crystalline material in the glass.
2. Instrument artifacts resulting from direct reflection of incident beam into spectrometer.
3. Unknown optical effects associated with use of small spherical specimens.

Because these effects have not yet been fully investigation, we limit the present paper to spectra without fine structure.

Composition of Glasses

Electron microprobe analyses of selected glass particles are listed in Table 1. Analyses for inhomogeneous glasses are shown as a range. The glasses, which are clearly separated into Ca-Al-rich regions and Fe-Mg-rich regions, are listed with an analysis of each region. Glasses with two or more phases are common, although only two phases are present in large quantity. Figure 1 shows the typical morphology of the biphasic glasses and the extent to which the two regions are interlocked. The

Fig. 1. Electron microprobe images of glass particle 14162,47–2C, showing zones of Ca, Al-rich and Fe-Mg-rich glass. Field of view is 180 × 180 μ.

heterogeneity of these samples creates difficulties for both Raman and x-ray emission spectroscopy because both utilize beams with about 100 μ spot sizes. The beam spans the entire sample area to give an average spectrum, whereas two distinct compositions and structures are present. The measured Al shifts for the biphasic glasses, however,

should be meaningful because the bulk of the Al contributing to the x-ray peak is contained in the Al-rich phase.

Many classifications of the parent rock type have now been proposed for the lunar fines. For the present work we have used the composition ranges of Reid *et al.* (1972). The separation into compositional populations by these workers is in general agreement with other analyses of lunar glasses (Glass, 1971; Prinz *et al.*, 1971; Apollo Soil Survey, 1971; Meyer *et al.*, 1971). The glasses selected for spectra measurement were assigned as derivatives of: (i) Mare basalts, (ii) Fra Mauro (KREEP) basalts, (iii) Highland (aluminum-rich basalts), and (iv) anorthosites. No particular attempt was made to separate out the several subtypes of Mare basalts because of the inhomogeneity of the specimens.

X-Ray Emission Spectra

All measurement on SiK_β, AlK_β, and OK_γ are given in Table 2. All shifts are in units of 10^{-4} angstroms with respect to the listed standard. Table 3 lists several relevant minerals for comparison. Jadeite and spodumene are included only to provide an AlK_β shift for aluminum in 6-coordination in a pyroxene host.

Table 2. X-ray emission shift data for lunar glasses.

Sample	αSiO_2 Std. SiK_β Δ (A $\times 10^{-4}$)	αAl_2O_3 Std. AlK_β Δ (A $\times 10^{-4}$)	αSiO_2 Std. OK_γ Δ (A $\times 10^{-4}$)
10084,110,1A (Green)	−15	+35	+262
10084,110,1B (Green)	−20	+16	+259
10084,110,2.8	−22	+37	+219
10084,110,2.9	−27	+36	−198
10084,110,III	−20	+23	+235
10084,110,3.1	−9	+35	+270
12070,42-1	−35	+35	+219
12070,42-2	−28	+36	+224
12070,42 3	−44	Insufficient Al	+235
12070,42 4	−25	+39	+256
12042,32-1	−26	+37	+222
12042,32-2	−28	+46	+187
12042,32 3	−34	+52	+200
12042,32-4	−29	+48	+184
14162,47-1	−39	+37	+227
14162,47-2B	−35	+36	+192
14162,47-2C	−25	+49	+182
14162,47-3	−44	+38	+206
14162,47-5	−40	+37	+171
14162,61-1	−42	+35	+208
14162,61-2	−38	+39	+214
14162,61 3	−49	+48	+206
14162,61 4	−37	+34	+214
14162,61 5	−31	+47	+216
15501,25	−39	+29	+240
15531,40	−52	No Al detected	+283
15231,49 1	−54	+21	+219
15231,49 2	−37	+35	+208
15231,49 3	−39	+30	+254
15015,26 (Rock)	−26	+49	+246
15017,9	−32	+34	+230
15245,56	−33	+37	+248

Table 3. X-ray emission shift data for reference minerals.

Sample	γSiO_2 Std. SiK_β Δ (A × 10^{-4})	γAl_2O_3 Std. AlK_β Δ (A × 10^{-4})	γSiO_2 Std. OK_γ Δ (A × 10^{-4})
Anorthite (Cry.)	−41	+24	+203
Anorthite (Glass)	−48	+39	+192
Amelia Albite	−14	+63	+136
Orthoclase	−15	+62	+120
Olivine	15	-	+219
Jadeite 1347	−26	+13	+112
Spodumene	−4	+14	+136

The span of SiK_β shifts covers much of the range known for silicate minerals (White and Gibbs, 1967). The Highland and Fra Mauro basalt glasses have only a small spread in their shift values. The averages and corresponding Si–O distances (scaled from White and Gibbs's plot) are

	SiK_β	Range	Si–O(Å)
Highland basalt glass	−24.4	(−15:−39)	1.621
Fra Mauro basalt glass	−38.5	(−35:−49)	1.630

There is a good correlation between SiK_β and the Si–O distance, because all Si is in 4-coordination. There is some ambiguity between Al coordination and Al–O distances if only AlK_β shift data are available. In contrast, the SiK_β shifts of the Mare basalts vary widely between specimens. The range of shifts is from −9 to −52, which corresponds to a range of Si–O distances of 1.612 to 1.637. Because most of the Mare basalt glasses examined were very inhomogeneous, this result is not surprising. Two of the largest shift values were found in grains 12070,42–3 and 15531,40, which had extremely low aluminum concentrations. All glasses with anorthositic compositions occurred as second phases with lower aluminum glasses, and no interference-free SiK_β shifts were measured for these glasses.

The AlK_β shifts are plotted against aluminum concentration in Fig. 2. The Fra Mauro basalt glasses fall into a narrow range, whereas there is a large scatter for the other compositions. The anorthosite glasses have definitely larger shifts than the more Fe-Mg-rich glasses. The means are

Anorthosite basalt glass	43.4
Fra Mauro basalt glass	35.5
Mare basalt glass	35.2
Highland basalt glass	32.0

The ranges are shown by the scatter of the data in Fig. 2. According to the criteria proposed by White and Gibbs (1969), the aluminum in the anorthosite composition glasses should be mainly in fourfold coordination. Some of the Highland and Mare basalt composition glasses have low AlK_β shifts, implying aluminum mainly in 6-coordination, whereas the bulk of the compositions fall into a range that would imply mixed aluminum coordination.

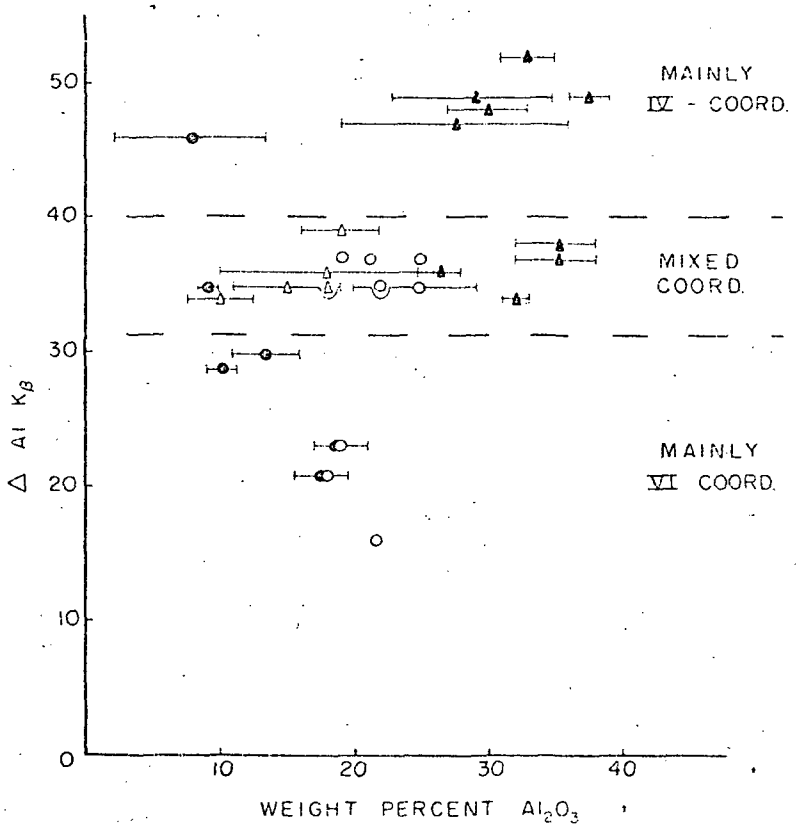

Fig. 2. X-ray emission shift for AlK_β (in units of 10^{-4} Å) plotted against aluminum concentration. Solid circles: Mare basalt compositions; open circles: Highland basalt compositions; open triangles: Fra Mauro basalt compositions; solid triangles: anorthosite compositions.

Raman Spectra

Representative Raman spectra of the lunar glasses are shown in Figs. 3, 4, and 5. The spectra consist of a variable number of weak bands, mostly broader than expected from crystalline materials and narrower than most spectra of synthetic glasses. In general, the spectra vary considerably from grain to grain and also from different spots on the same grain, as might be expected from such heterogeneous samples. Although the overall spectra have a wide range, certain bands reappear consistently throughout the data. The spectra can be discussed in terms of four regions: 100 cm^{-1}, 400 to 800 cm^{-1} containing mainly bending motions of silicate structural units and stretching motions of octahedrally coordinated structural units, 800 to 1100 cm^{-1} containing stretching motions of SiO_4 tetrahedra, and the region above 1200 cm^{-1}.

The 800 to 1100 cm^{-1} region contains a commonly recurring band in the range of 1002 to 1006 cm^{-1}, a pair of bands at 819 to 823 and 850 to 853 cm^{-1}, and a few

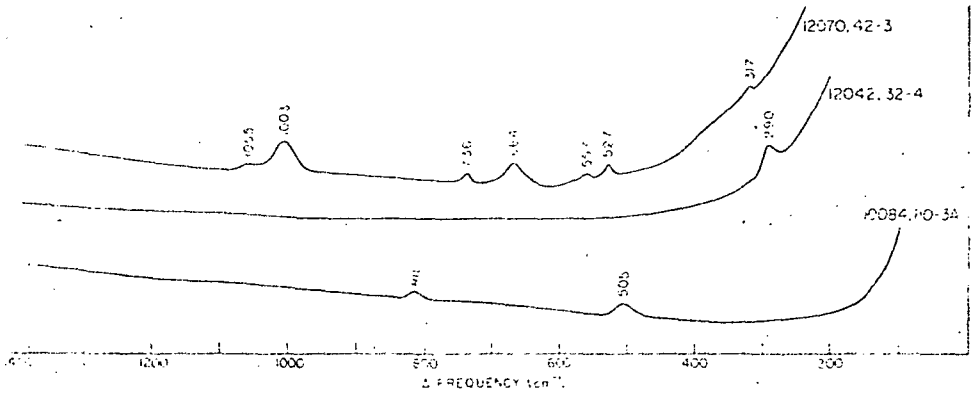

Fig. 3. Raman spectra of Apollo 11 and 12 glasses.

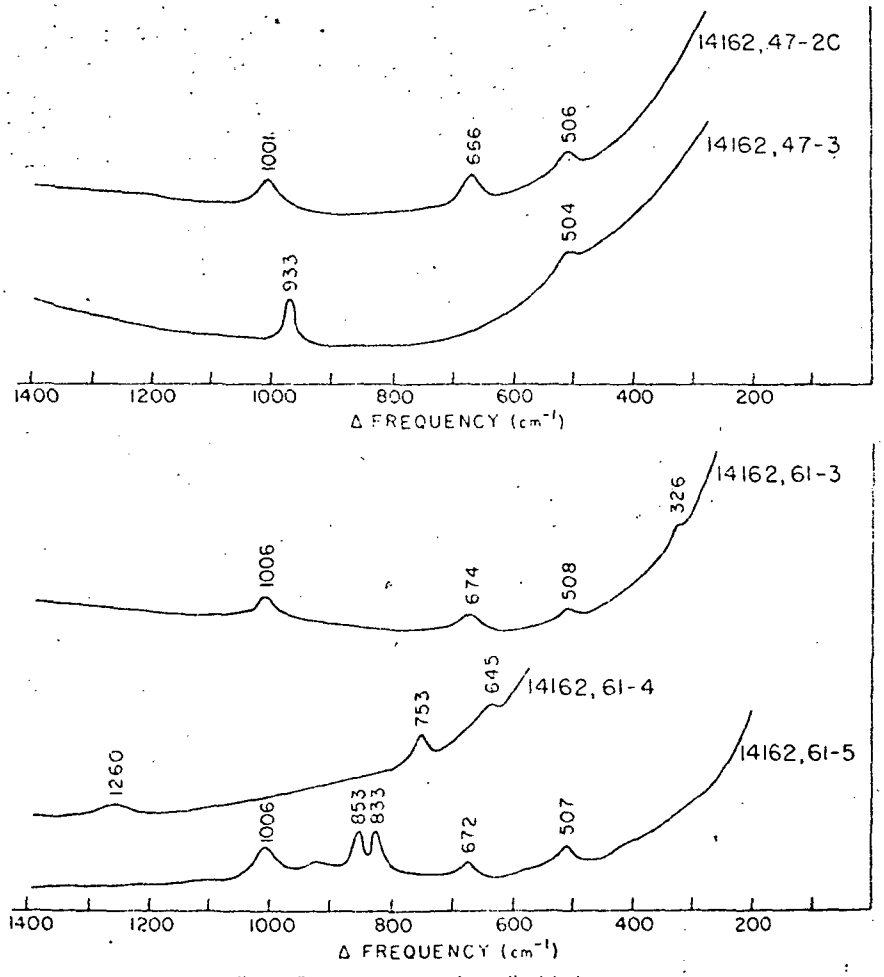

Fig. 4. Raman spectra of Apollo 14 glasses.

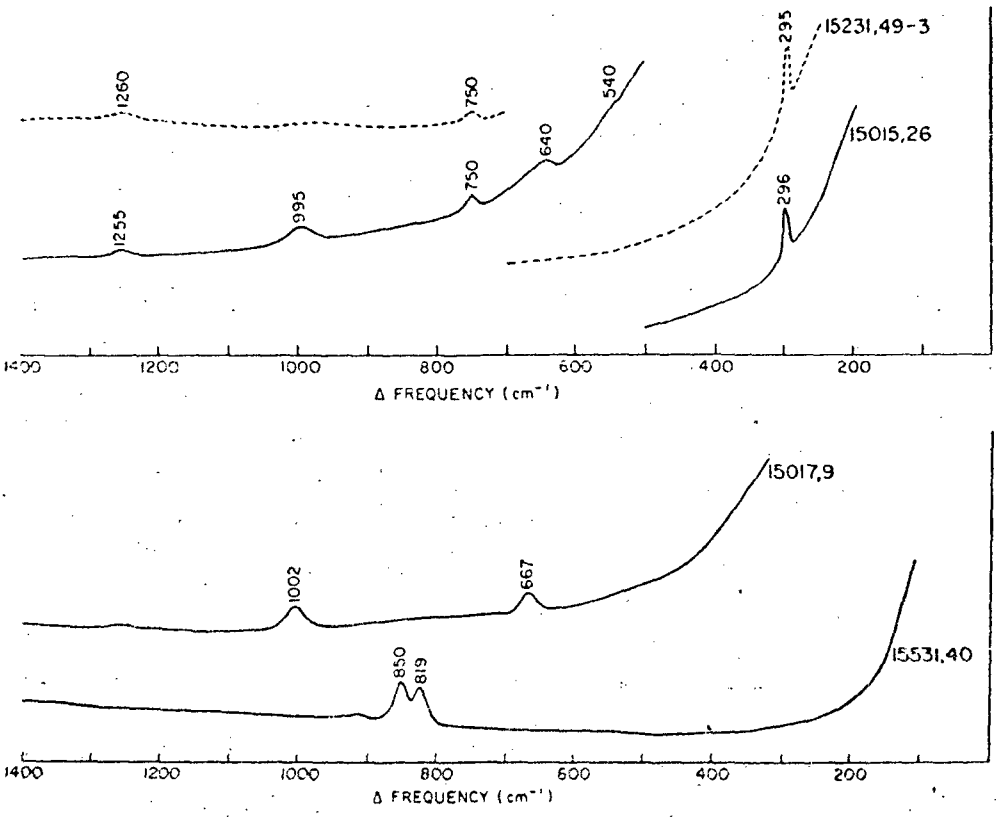

Fig. 5. Raman spectra of Apollo 15 glasses.

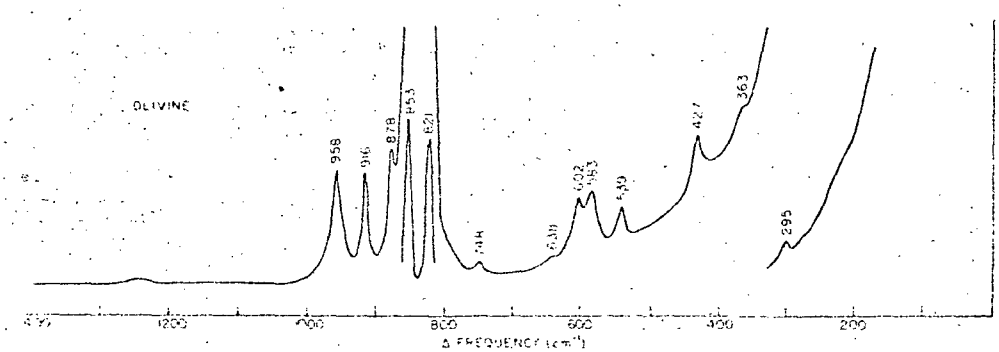

Fig. 6. Raman spectrum of polycrystalline olivine.

other less systematic bands. The 820 to 850 pair in particular seems unusually sharp for glass spectra. There is a good correlation between these bands and the stretching frequencies of olivine and pyroxene. Spectra of powder olivine and four pyroxenes are shown in Figs. 6 and 7. The strongest bands in the olivine spectrum are the two at 821 and 853. All pyroxene spectra contain a sharp band in the range of 1000 to

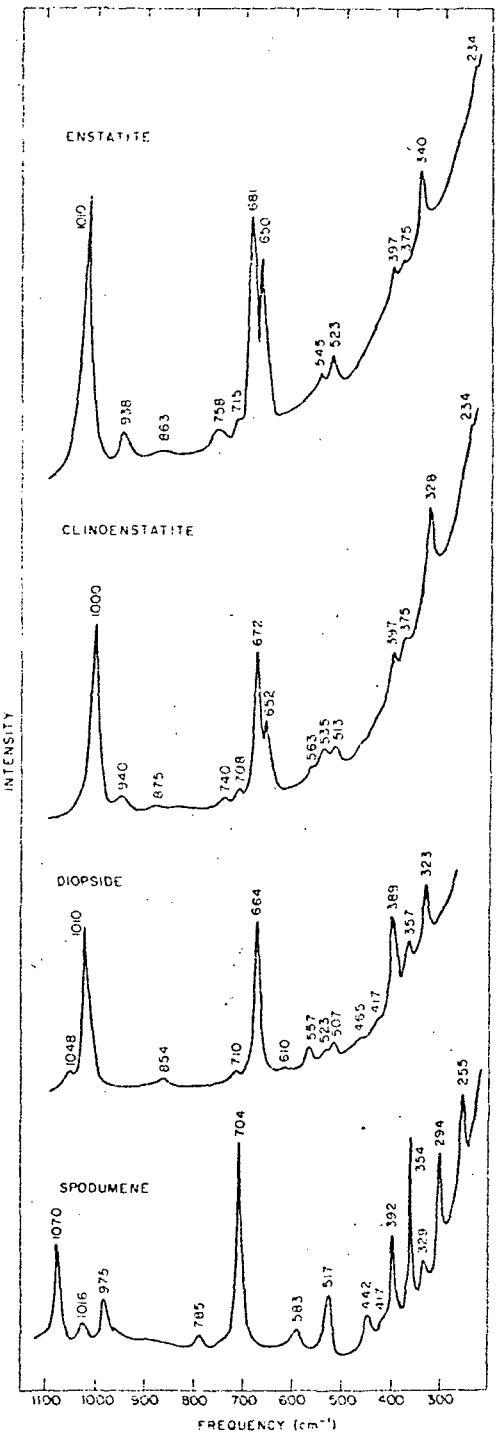

Fig. 7. Raman spectra of polycrystalline pyroxene.

1010 cm^{-1} in close agreement with the glass spectra. The second strongest band occurs as a doublet in the 650 to 670 cm^{-1} region for enstatite and clinoenstatite and as a single band at 664 in diopside. A band occurs in this frequency range for each specimen for which the 1002 to 1006 cm^{-1} band appears. However, these bands are broadened, and there is little evidence for doublet structure.

The other crystalline or quasi-crystalline phase that might contribute to the spectra is feldspar, particularly in those glasses with anorthosite composition zones. Because of the low alkali content of the lunar glasses, anorthite is the only feldspar likely to be present. Raman spectra for three end-members feldspars are shown in Fig. 8. The alkali feldspars have a strong band at 506 to 513 cm^{-1}, but the corresponding band in anorthite is relatively weak. The agreement between this frequency of the crystalline feldspars and the 506 to 508 band in the lunar glass spectra is rather good. The Si–O stretching frequencies of the feldspars are all weak and do not appear in the glass spectra.

The broad band at 1250 to 1260 cm^{-1} that appears in several of the spectra is difficult to interpret. It also appeared in the spectra of Apollo 11 glasses reported earlier (White *et al.*, 1971). This band is in the correct frequency range to be due to tetrahedral stretching vibrations but lies at a higher frequency than any Si–O vibra-

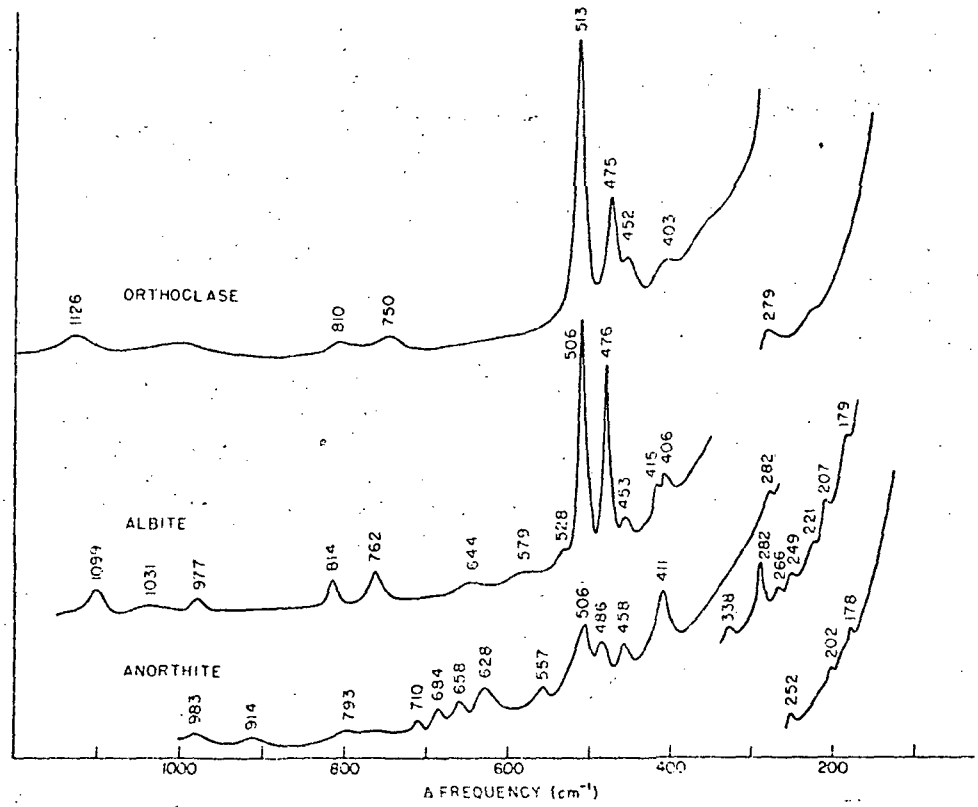

Fig. 8. Raman spectra of polycrystalline feldspars.

tions so far observed. When the Si--O stretching frequencies for olivine, pyroxene, and feldspar are compared, it is apparent that the Raman frequencies increase from 850 to 1000 to 1100 to cm^{-1} as the amount of corner linking of the tetrahedra increases. A similar effects in the infrared spectra of silicates has long been known. The highest-frequency mode in the feldspar structures with complete corner sharing is 1126 cm^{-1}; and the highest frequency in quartz is 1162 cm^{-1} (Scott and Porto, 1967).

The Raman spectra of the lunar glasses contain bands from the following sources:

1. Submicroscopic crystalline inclusions of olivine and pyroxene.
2. Regions of the glass in which there is incipient crystallization to one of the silicate mineral phases. These give rise to the strong bands characteristic of the mineral but with considerable band broadening.
3. Broad bands characteristic of the glass itself, most important of these in the 1260 cm^{-1} that may represent the Si-O stretching frequency of glass of higher density.

Acknowledgments This work was supported under NASA Grant NGR-39-009(152) and through the Space Sciences and Engineering Laboratory of the Pennsylvania State University operated under NASA Grant NGL 39-009-015.

References

Apollo Soil Survey (1971) Apollo 14: Nature and origin of rock types in soil from the Fra Mauro formation. *Earth Planet. Sci. Lett.* **12**, 49–54.

Gigl P. D. Savanick G. A. and White E. W. (1970) Characterization of corrosion layers on aluminum by shifts in the aluminum and oxygen x-ray emission bands. *J. Electrochem. Soc.* **117**, 15–17.

Glass B. P. (1971) Investigation of glass recovered from Apollo sample 12057. *J. Geophys. Res.* **76**, 5649–5657.

Meyer C. Jr. Brett R. Hubbard N. J. Morrison D. A. McKay D. S. Aiken F. K. Takeda A. and Schonfeld E. (1971). Mineralogy, chemistry and origin of the KREEP component in soil samples from the Ocean of Storms. *Proc. Second Lunar Sci. Conf., Geochim. Cosmochim. Acta* Suppl. 2, Vol. 1, pp. 393–411. MIT Press.

Prinz M. Bunch E. E. and Keil K. (1971) Composition and origin of lithic fragments and glasses in Apollo 11 samples. *Contrib. Mineral. Petrol.* **32**, 211–230.

Reid A. M. Ridley W. I. Warner J. Harmon R. S. Brett R. Jakeš P. and Brown R. (1972) Chemistry of Highland and Mare basalts as inferred from glasses in the lunar soils (abstract). In *Lunar Science—III* (editor C. Watkins), p. 640. Lunar Science Institute Contr. No. 88.

Scott J. F. and Porto S. P. S. (1967) Longitudinal and transverse optical lattice vibrations in quartz. *Phys. Rev.* **161**, 903–910.

White E. W. and Gibbs G. V. (1967) Structural and chemical effects on the SiK_β x-ray line for silicates. *Amer. Mineral.* **52**, 985–993.

White E. W. and Gibbs G. V. (1969) Structural and chemical effects on the AlK_β x-ray emission band among aluminum-containing silicates and aluminum oxides. *Amer. Mineral.* **54**, 931–936.

White W. B. White E. W. Görz H. Henisch H. K. Fabel G. W. Roy R. and Weber J. N. (1971) Physical characterization of lunar glasses and fines. *Proc. Second Lunar Sci. Conf., Geochim. Cosmochim. Acta* Suppl. 2, Vol. 3, pp. 2213–2224. MIT Press.

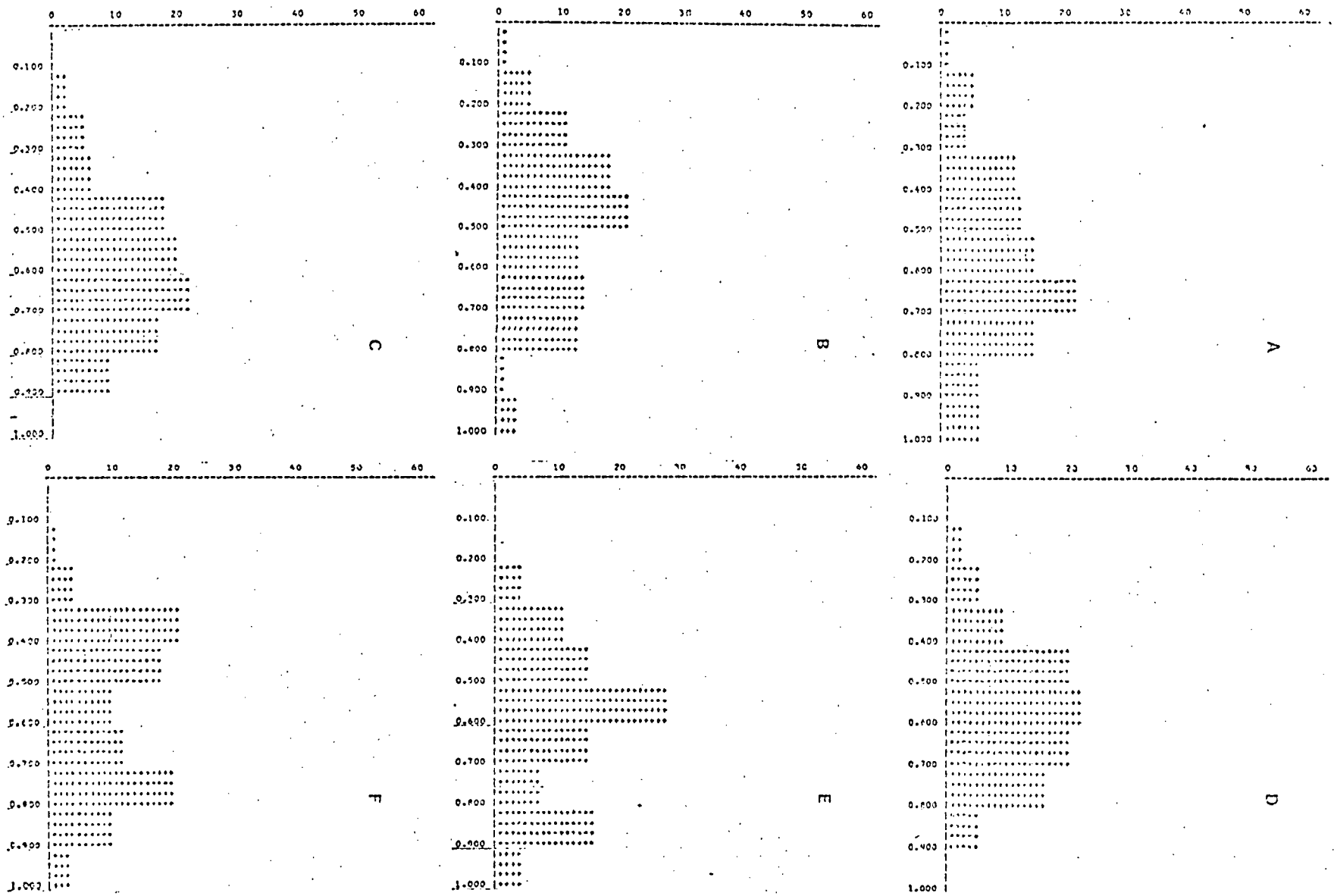
0
10
20
30
40
50
60
0.100
0.200
0.300
0.400
0.500
0.600
0.700
0.800
0.900
1.000
C
B
A
F
E
D

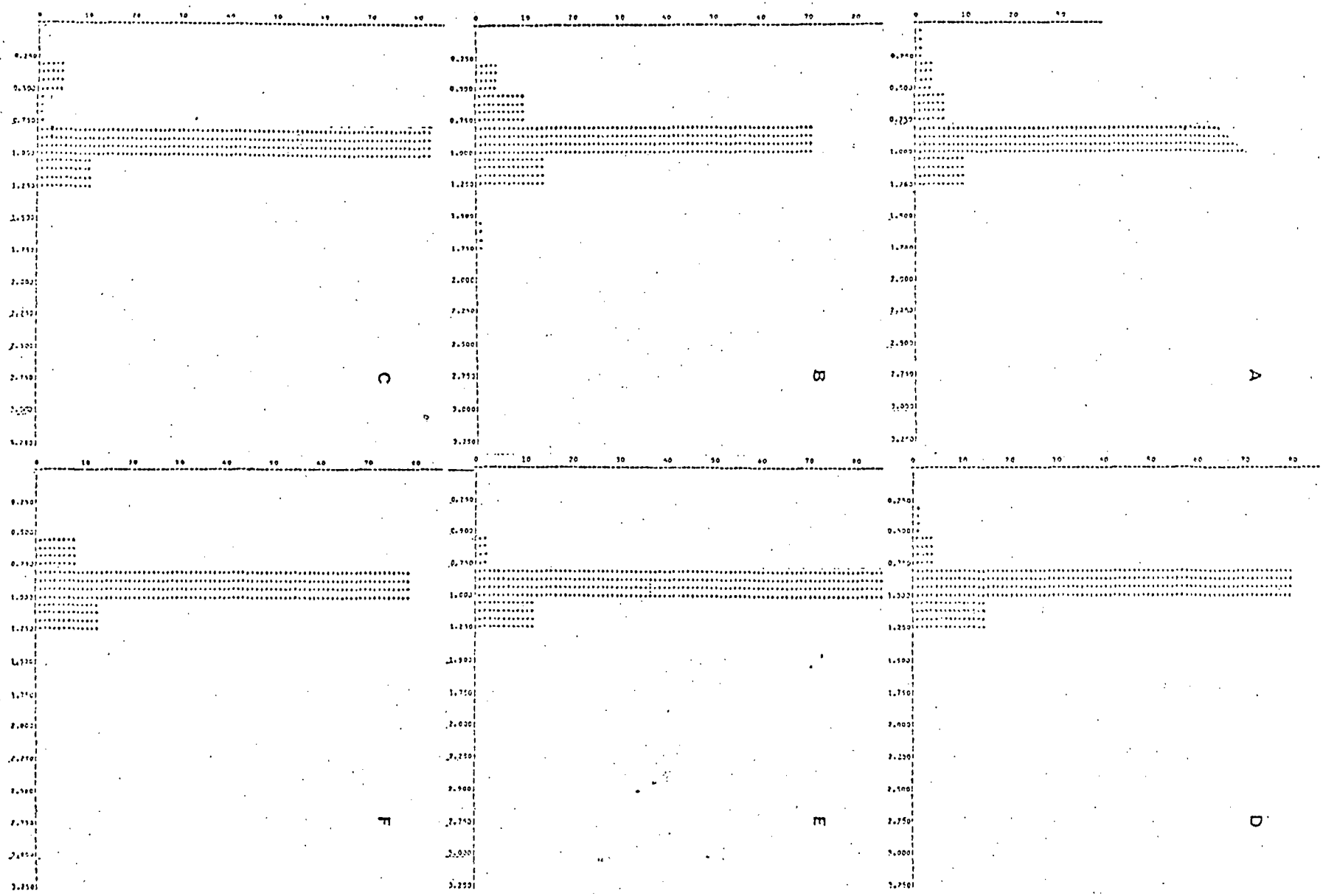
C
B
A
F
E
D

INTRODUCTION

This report is an interim one-year summary of the work carried out by the lunar sample team of the Materials Research Laboratory of The Pennsylvania State University. Most effort was focused on the Apollo 14 samples which arrived in mid-1971 and the Apollo 15 samples which arrived in late 1971. The most important aspects of this work were reported at the Third Lunar Science Conference and the complete papers, to be published in the Conference Proceedings, are appended to this report.

Research on the structure and properties of lunar glass and synthetic analogs has also been supported through the Universities Space Science and Engineering Laboratory under NASA Institutional Grant 39-009-15.

RESULTS REPORTED TO THE LUNAR SCIENCE CONFERENCE

Two aspects of the physical characterization of lunar fines and glasses were presented. The titles of the papers were:

"Structure of lunar glasses by Raman and soft x-ray spectroscopy" by G. W. Fabel, W. B. White, E. W. White and R. Roy.

"CESEMI studies of Apollo 14 and 15 fines" by H. Görz, E. W. White, G. G. Johnson, Jr., and M. W. Pearson.

Both papers have been accepted for publication in the Conference Proceedings. Work along these lines is continuing particularly on the Apollo 15 samples which arrived only a few weeks before the Lunar Science Conference.

OTHER RESEARCH CURRENTLY UNDERWAY

1. Electronic Spectra of Lunar Glass

The role of iron and titanium in explaining the optical properties of lunar minerals and glasses is still a largely unresolved

problem. We are currently making measurements of the optical absorption spectra of glass particles from the Apollo 14 and 15 samples. The correlation of absorption features with specific transitions in iron and titanium ions is, however, difficult because of the unknown effects of electron transfer absorption. To provide a background for spectra assignments we are preparing synthetic glasses of anorthite and highland basalt composition but continuing either iron, titanium, or iron + titanium in known concentrations and are melting the glasses under various known oxygen fugacities. Optical spectra of the synthetic glasses will then be measured.

2. Raman Spectra of Terrestrial Glasses

A wealth of new information has been uncovered by measurement of Raman spectra of lunar glasses. Unfortunately this tool is so new that little is known about the Raman spectra and their interpretation of any glasses. As a result, the application to the structurally and compositionally more complex lunar glasses is difficult. To provide part of this information we have assembled a suite of terrestrial glasses, obsidians, fulgarites, and tekties for spectral measurement. The chemical compositions have been determined by electron probe and both Raman and Soft-X-ray spectra are now being measured.

STRUCTURE OF LUNAR GLASSES BY RAMAN AND SOFT X-RAY SPECTROSCOPY

George W. Fabel, William B. White, Eugene W. White and Rustum Roy

CESEMI STUDIES OF APOLLO 14 AND 15 FINES

Herta Görz, E. W. White, G. G. Johnson, Jr. and Mary W. Pearson

CESEMI Studies of Apollo 14 and 15 Fines

HERTA GÖRZ, E.W. WHITE, G.G. JOHNSON, JR., and MARY W. PEARSON
Materials Research Laboratory, The Pennsylvania State University,
University Park, Pennsylvania 16802

Abstract - Quantitative size and shape analyses have been carried out on six lunar fines from Apollo 14 and 15 by computer evaluation of scanning electron microscope images (CESEMI). For the size range of 0.50 to 30 μm diameter, the distributions are log-normal on a number count basis. This finding is in contrast with results for coarser materials in the fines reported by King et al. suggesting the operation of a different process. Aspect ratios range from 0.1 to 1.0 with an average value of about 0.6. Only slight differences are observed among samples. A shape complexity factor (ratio of particle perimeter to ellipse perimeter) also varies only slightly among the six samples.

INTRODUCTION

The CESEMI technique (Computer Evaluation of Scanning Electron Microscope Images) permits the size, shape and chemical analysis of fine particles in the micron and submicron range (McMILLAN et al., 1969; WHITE et al., 1970; GÖRZ et al., 1971). This paper presents results on the size and shape analysis of six lunar fines including sample 14163,158, 15031,44, 15041,50, 15231,49, 15501,25, 15531,40. The purpose of this study is to determine the shape of the grain size distribution curve in the lower particle size range (0.5-30μm) which cannot be readily done by other means. Several authors (FRONDEL et al., 1971; HEYWOOD, 1971; KING et al., 1971; SELLERS et al., 1971) have published size distribution curves derived from weight determinations by sieving and Coulter counting techniques. The lower cut-off of those curves occurs at around 2-10μm, a size range where the scanning electron microscope technique is helpful in describing the finer grain sizes.

The microscopical studies of the six fines indicate an upper size limit of around 600μm, the shape of the particles ranging from spherical (brown glass, seldom) to angular with sharp edges. The minerals identified were pyroxene (greenish brown, sharp edges, sometimes isotropic), olivine (green to brown, rounded), plagioclase (sometimes twins, optical character negative), opaques, and glasses with various colors, shapes and refractive indices. The amount of glasses in these samples is higher than in the samples of Apollo 11 and 12 studied. It is remarkable that the appearance of the glass fragments regarding color and shape resembles very often that of clinopyroxene. Only very few glass spheres or dumbbells have been found.

SPECIMEN PREPARATION AND RECORDING PARAMETERS

The medium for dispersing the fines on a substrate for the CESEMI recordings is a eutectic mixture of camphor and naphthalene (THAULOW and WHITE, in press). For this study, highly polished metallic Be was chosen as a substrate. The samples were not given a conductive coating. The secondary electron images were recorded using a voltage of 25 keV and 10^{-9} amp specimen current. The secondary electron detector was optimized to suppress shadows. All images were recorded at a picture point density of 256 points per line and 256 lines. Six images were recorded for each of the six samples; three were taken at 300X, three at 1250X magnification.

RESULTS AND DISCUSSION

In order to accurately measure the size distribution over the range of 0.5 to 30μm, data from the two magnification settings had to be combined, taking into account the relative areas represented by the two magnifications. The data were merged with no overlap between magnifications. For the magnifications 300X and 1250X the following limits were used (Table 1):

Table 1. Limits for merging

Magnification	Lower size limit	Upper size limit
1250X	0.5μm	5.0μm
300X	5.0μm	30.0μm

The number of counts must be weighted to account for the relative areas sampled. The area sampled at 1250X is approximately 1/17 that of the area sampled at 300X, hence the number of counts are adjusted accordingly.

Results of the particle size analyses are summarized in the Figures 1 and 2. On the logarithmic scale is recorded the equivalent circular diameter of the particles; on the probability scale the cumulative frequency of the number of grains. The size distributions are essentially log-normal. Because of the selected cut-offs discussed above, the smallest grain size counted is 0.5μ. A slight uncertainty due to statistics of the counting is evidenced in the upper size range (above 98%).

Table 2 presents the total number of grains processed for establishing the frequency curves, the median size of the equivalent circular diameter, and the slope of the distribution curves mathematically fitted for data between 5% and 95% probability.

Table 2. Number of particles, median size of merged equivalent circular diameter, and slope of distribution curves for six lunar fines.

Sample	Number of particles measured	Median size of equivalent circular diameter (μm)	Slope of distribution curve
14163,158	471	0.90	0.97
15031,44	603	0.86	0.97
15041,50	220	0.84	0.91
15231,49	365	1.37	0.89
15501,25	195	1.17	1.09
15531,40	157	1.49	0.92

The shapes of the particles in the size range of 1.25-30μm equivalent circular diameter were characterized from ellipses calculated by least square fits to each particle perimeter (MATSON et al., 1970). Histograms of the aspect ratios (minor/major axes of calculated ellipses) are given in Fig. 3. An aspect ratio of 1.0 indicates an equant particle, while a ratio of 0.1 indicates an elongate shape. Most grains seem to be slightly-to-medium elongated with a ratio between 0.4-0.7. Samples 15501 and 15531 show bimodal distributions.

Figure 4 summarizes the histograms of the shape complexity factor (particle perimeter/fitted ellipse perimeter). Around 80% of the grains measured have a shape complexity factor in the range 0.80-1.00. If a particle has a shape complexity factor of greater than 1, then the particle is highly angular and complex with possible reentrant perimeter. If the factor is equal to 1, the particle is smooth and not reentrant, while a factor less than 1 shows an extremely regular particle but not elliptical in shape.

CONCLUSIONS

The six samples of lunar fines used in this study all have size distributions that are log-normal on a number count basis over the size range from 0.5 to 30μm. All six distribution curves have the same slope. As the distributions are log-normal on a number count basis they are, of necessity, nonlog-normal on a weight basis. This finding is quite different than King et al. found for the coarser fractions where they find log-normal behavior on a weight basis.

Sellers et al. interpret the log-normal behavior (weight basis) to be indicative of communition processes. Since we observe a different distribution function for the finer fraction (0.5-30μm) one can only assume that different processes are operative in generating these fine particles.

Acknowledgment - This work was supported under NASA Grant NGR-39-009-183.

REFERENCES

FRONDEL C., KLEIN C. JR., and ITO J. (1971) Mineralogical and chemical data on Apollo 12 lunar fines. Proc. Second Lunar Sci. Conf., Geochim. Cosmochim. Acta Suppl. 2, Vol. 1, pp. 719-726. MIT Press.

GÖRZ H., WHITE E.W., ROY R., and JOHNSON G.G., JR. (1971) Particle size and shape distributions of lunar fines by CESEMI. Proc. Second Lunar Sci. Conf., Geochim. Cosmochim. Acta Suppl. 2, Vol. 3, pp. 2021-2025. MIT Press.

HEYWOOD H. (1971) Particle size and shape distribution for lunar fines sample 12057,72. Proc. Second Lunar Sci. Conf., Geochim. Cosmochim. Acta Suppl. 2, Vol. 3, pp. 1989-2001. MIT Press.

KIM Y.K., LEE S.M., YANG T.H., KIM T.H., and KIM C.K. (1971) Mineralogical and chemical studies of lunar fines 10084,148 and 12070,98. Proc. Second Lunar Sci. Conf., Geochim. Cosmochim. Acta Suppl. 2, Vol. 1, pp. 741-755 MIT Press.

MATSON W.L., McKINSTRY H.A., JOHNSON G.G., JR., WHITE E.W., and McMILLAN R.E. (1970) Computer processing of SEM images by contour analyses. Pattern Recognition 2, 303-312.

McKAY D.S., MORRISON D.A., CLINTON U.S., LADLE G.H., and LINDSAY J.F. (1971) Apollo 12 soil and breccia. Proc. Second Lunar Sci. Conf., Geochim. Cosmochim. Acta Suppl. 2 Vol. 1, p. 755-776. MIT Press.

McMILLAN R.E., JOHNSON G.G., JR., and WHITE E.W. (1969) Computer processing of binary maps of SEM images. Second Annual Scanning Electron Microscope Symposium, IITRI, 439-444.

SELLERS G.A., WOO C.C., and BIRD M.L. (1971) Composition and grain-size characteristics of fines from the Apollo 12 double-core tube. Proc. Second Lunar Sci. Conf., Geochim. Cosmochim. Acta Suppl. 2, Vol. 1, pp. 665-678. MIT Press.

THAULOW N. and WHITE E.W. General method for dispersing and disaggregating particulate samples for quantitative SEM and optical microscope studies (to be published in Powder Technology).

D

WHITE E.W., GÖRZ H., JOHNSON G.G., JR., and McMILLAN R.E. (1970) Particle size distributions of particulate aluminas from computer processed SEM images. Third Annual Scanning Electron Microscope Symposium, IITRI, 57-64.

WHITE E.W., MAYBERRY K., and JOHNSON G.G., JR. Computer analysis of multi-channel SEM and X-ray images from fine particles (to be published in Pattern Recognition).

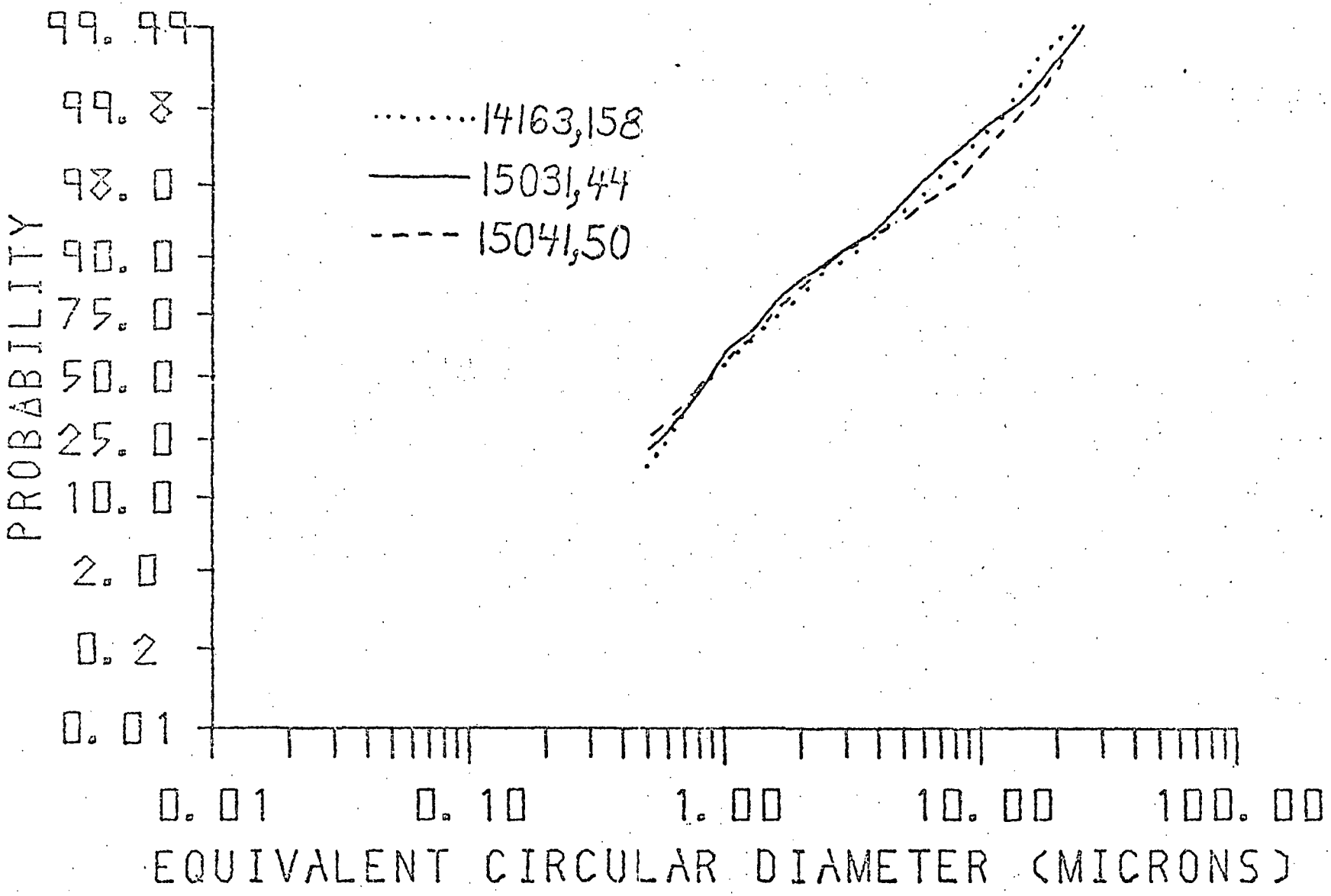
99.99
99.8
98.0
90.0
75.0
50.0
25.0
10.0
2.0
0.2
0.01
PROBABILITY
14163,158
15031,44
15041,50
0.01
0.10
1.00
10.00
100.00
EQUIVALENT CIRCULAR DIAMETER (MICRONS)

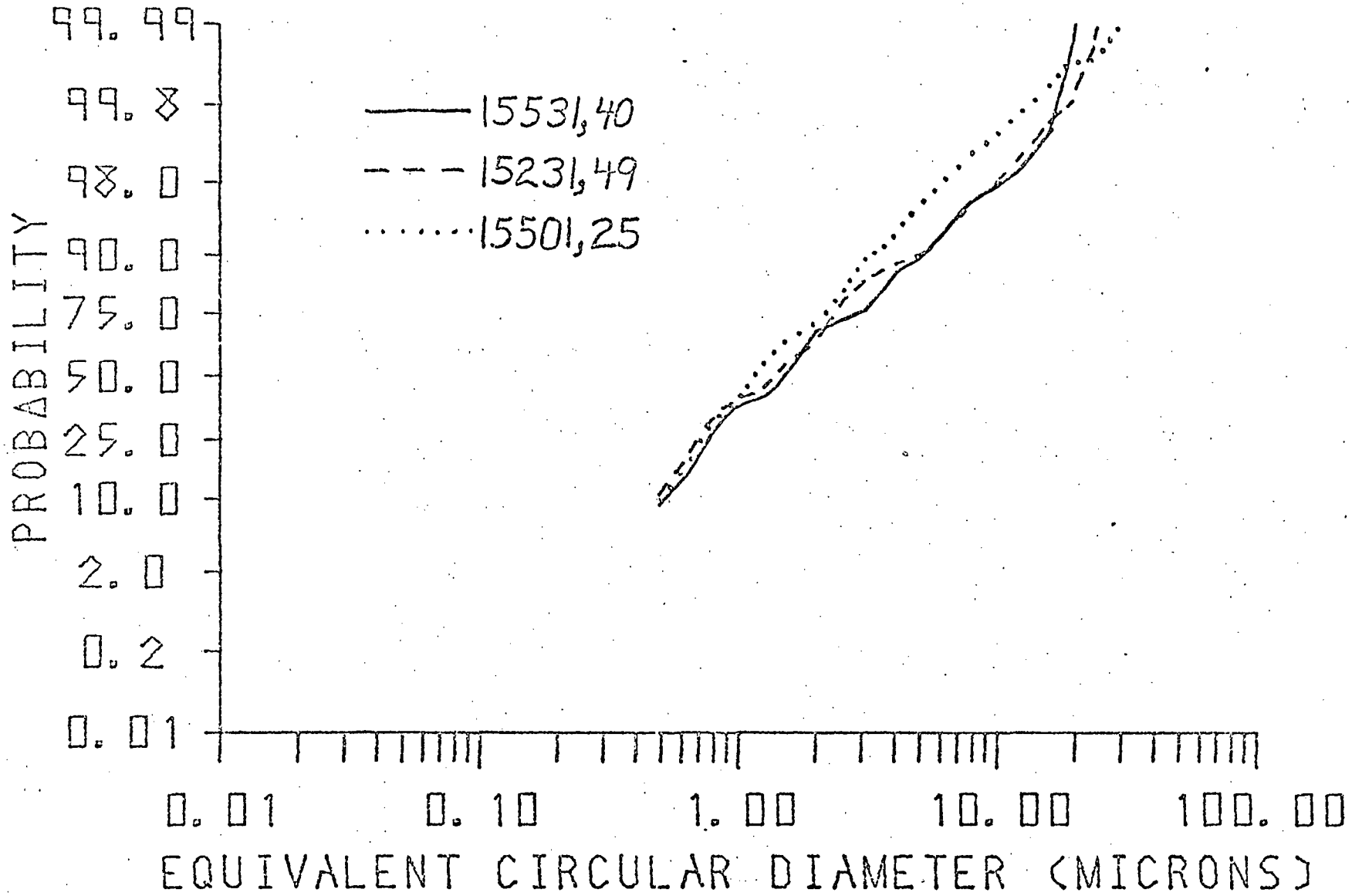
99.99
99.8
98.0
90.0
75.0
50.0
25.0
10.0
2.0
0.2
0.01
PROBABILITY
15531,40
15231,49
15501,25
0.01
0.10
1.00
10.00
100.00
EQUIVALENT CIRCULAR DIAMETER (MICRONS)

CAPTIONS FOR FIGURES

Figure 1. Cumulative frequency versus equivalent circular diameter for three lunar fines.

Figure 2. Cumulative frequency versus equivalent circular diameter for three lunar fines.

Figure 3. Frequency in percent versus the aspect ratio (minor/major axis of calculated ellipse) for six lunar fines.

a. Sample 14163,158
b. Sample 15031,44
c. Sample 15041,50
d. Sample 15231,49
e. SAmple 15501,25
f. Sample 15531,40

Figure 4. Frequency in percent versus shape complexity factor (ratio of particle perimeter to ellipse perimeter) for six lunar fines.

a. Sample 14163,158
b. Sample 15031,44
c. Sample 15041,40
d. Sample 15231,49
e. Sample 15501,25
f. Sample 15531,40